Identification of the elastic constant values for numerical simulation of high velocity impact on Dyneema ® woven fabrics using orthogonal experiments

DOI:
10.1016/j.compstruct.2018.07.024

Document Version
Accepted author manuscript

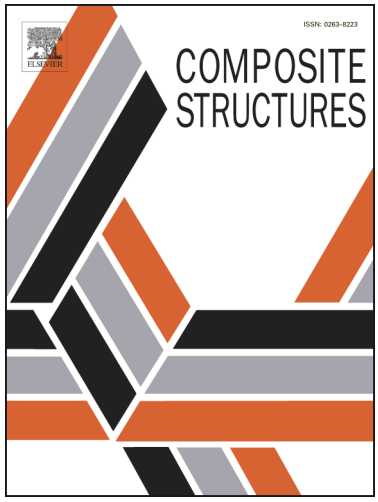

Identification of the elastic constant values for numerical simulation of high velocity impact on Dyneema® woven fabrics using orthogonal experiments

Zishun Yuan, Xiaogang Chen, Haoxian Zeng, Kaicheng Wang, Jiawen Qiu

PII: S0263-8223(17)32089-5
DOI: https://doi.org/10.1016/j.compstruct.2018.07.024
Reference: COST 9941

To appear in: *Composite Structures*

Received Date: 5 July 2017
Revised Date: 10 May 2018
Accepted Date: 4 July 2018

Please cite this article as: Yuan, Z., Chen, X., Zeng, H., Wang, K., Qiu, J., Identification of the elastic constant values for numerical simulation of high velocity impact on Dyneema® woven fabrics using orthogonal experiments, *Composite Structures* (2018), doi: https://doi.org/10.1016/j.compstruct.2018.07.024

Identification of the elastic constant values for numerical simulation of high velocity impact on Dyneema® woven fabrics using orthogonal experiments

Zishun Yuan, Xiaogang Chen*, Haoxian Zeng, Kaicheng Wang, Jiawen Qiu
School of Materials, University of Manchester, Manchester, UK M13 9PL

*Corresponding author. Email: xiaogang.chen@manchester.ac.uk

Abstract:

Dyneema® fibres and fabrics are widely used for ballistic protection due to its lightweight and super mechanical properties against high strain rate impact, and finite element (FE) simulation and analysis are used to study the response to the impact in parallel to the experimental-based research methods. However, elastic constants of the yarn except the Young's modulus were difficult to obtain and were basically assigned based on assumptions and approximations in the FE modelling, which caused some inaccuracies. This paper reports a study on the influence of each elastic constant of Dyneema® yarn model in modelling a single layer Dyneema® woven fabric against ballistic impact using the orthogonal experiment method. Orthogonal table L_{25} (5^6) was employed to analyse six factors (*i.e.* E_{11}, E_{33}, ν, G_{13}, G_{23}, and their interactions) with each having five levels. The ballistic modelling results were validated against the experimental results, *viz.* energy absorption, failure time of the first yarn broken and number of failed yarns. According to the orthogonal analysis, G_{13} was shown as the most significant in influencing the simulated results, with a confidence level of more than 95%, and ν was the least significant. Through the orthogonal study, the combination of levels of the elastic constants that led to a significant agreement between the FE and practical results was identified.

Key words: Dyneema® yarn; elastic constants; orthogonal experiment; ballistic impact; woven fabric

1. Introduction

Finite element method (FEM) is a widely used for prediction and analysis of materials and structures for ballistic protection. It facilitates a deep and comprehensive understanding of the material responses, and would lead to the improvement of the materials. However, developing a reliable FE model demands several inevitable steps, one of them being to define properties to the material with accuracy [1].

Ultra-high molecular-weight polyethylene (UHMWPE) yarn (*e.g.* Dyneema® and Spectra®) is one of the most widely man-made yarns for ballistic protection due to its lightweight and super mechanical properties against high strain rate impact. Finite element (FE) simulation and analysis are used to study the response to the impact in parallel to the experimental-based

research methods. However, the elastic constants of a yarn in a woven fabric, as shown in Figure 1, were difficult to obtain except the Young's modulus and were basically assigned based on assumptions and approximations in the FE modelling, which caused some inaccuracies. The elastic constants associated to a yarn includes the longitudinal Young's modulus E_{11}, transverse moduli E_{22} and E_{33}, shear moduli G_{12}, G_{13} and G_{23}, and Poisson's ratios ν_{12}, ν_{13} and ν_{23}.

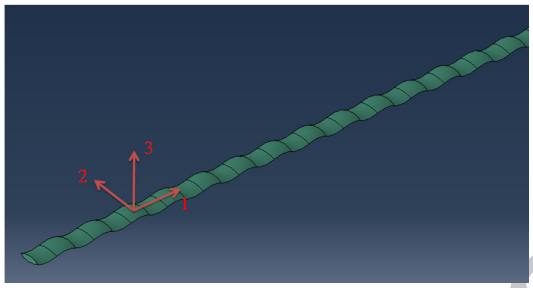

Figure 1. Directions of a yarn

Young's modulus of yarns in the longitudinal direction was basically obtained experimentally [2], and the modulus value is dependent on the strain rate. For high strain rate tensile tests, Huang *et al.* [3] measured 80GPa of the Young's modulus of UHMWPE fibre bundles at a high strain rate of 700/s while Koh *et al.* [4] did the same test for the same type of yarn at strain rate of 10^2/s, measuring approximately 120GPa of its Young's modulus. However, Russell *et al.* [5] considered the Young's modulus of the UHMWPE yarns to be slightly higher than 120GPa according to their tensile tests at strain rates from 10^{-1}/s to 10^3/s. For FE modelling of high speed impact, Grujicic *et al.* [6] specified 118GPa to the Young's modulus of UHMWPE yarn for simulating the ballistic performance of its composites model at impact velocities from 600m/s to 900m/s. Min *et al.* [7] defined 112GPa to the Young's modulus of Dyneema® yarn and Zhou *et al.* [8] assigned it to be 130GPa. The impact speed in the two studies was at around 500m/s. Chocron *et al.* [9] assigned 95GPa to the Young's modulus of Dyneema® yarn to simulate Dyneema® woven fabric model at impact speed of 477m/s.

Whilst value of the Young's modulus came from measurement**,** the other elastic constants were difficult to obtain and were usually defined on the basis of approximations and assumptions. Min *et al.* [7] assumed that Dyneema® yarn was isotropic, following the study of Wang *et al.* [10] who worked on Kevlar® fabric. Zhou *et al.* [8] treated the Dyneema® yarn model as a transversely isotropic material. The transverse moduli (E_{22} and E_{33}) of Dyneema® yarn in this study [8] were both assigned to be 1.21GPa, according to the experimental results of Dyneema® fibre obtained by Kawabata [11], and the shear moduli (G_{12} and G_{13}) were set to be 3.28GPa that was proposed by Grujicic [12] for Kevlar® yarns. In addition, Grujicic *et al.* [6] assumed that all of the Dyneema® yarn's transverse moduli (E_{22} and E_{33}) and shear moduli (G_{12}, G_{13} and G_{23}) were identical to 6.00GPa, which was approximately 1/20 of its longitudinal modulus. The assumption made by Chocron *et al.* [9] for the Dyneema® yarn's transverse moduli (E_{22} and E_{33}) was that it was an order of magnitude smaller than its longitudinal modulus, and that for the shear moduli (G_{12}, G_{13} and G_{23}) were two orders smaller than the longitudinal modulus. In these four studies above [7-9][12], the impact velocities were in the range from 400m/s to 600m/s.

The casual assignment of the elastic constant values for FE simulation caused concerns from many researchers, whether the UHMWPE fibre or aramid fibre were used for the fabrics. Nilakantan [13] studied the effect of transverse modulus and shear modulus of Kevlar KM2® fibre on the ballistic behaviours of the filament-level yarn models, and demonstrated that both moduli had significant influence on the ballistic performance of the yarn model. Sockalingam *et al.* [14] simulated the ballistic events with shear modulus being 1.8GPa and 24.4GPa, where Kevlar® KM2 yarn was subject to transverse impact. The results indicated that fibre failure was very sensitive to shear modulus. Ha-Minh *et al.* [15] studied the effect of transverse modulus, shear modulus and Poisson's ratio of a two-dimensional Kevlar KM2® yarn model on the ballistic performance of the yarn and fabric model. They concluded that shear modulus played a significant role on the ballistic behaviours of Kevlar KM2® yarn and fabric models. However, in these studies [13-15], they only investigated on the influence on the alteration of simple factor, which were not sufficient to show the influence of each constant in the whole elastic system. Komeil *et al.* [16, 17], Akmar *et al.* [18], and Erol *et al.* [19] recently applied the design-of-experiments approach to identify the influence of multiply mesoscale material properties in woven fabric models, and obtained the significance of each property.

This paper aims to reveal the sensitivity of the elastic constants on the ballistic response using the orthogonal experimental method. Optimisations are to be carried out to identify the values of the most sensitive elastic constants, to be used for simulating the ballistic performance of Dyneema® fabrics. The experimental results, *viz.* energy absorption, failure time of the first yarn broken, and the number of failed yarns, will be used as criteria to evaluate the ballistic performance of the model. This study is set to provide a feasible procedure of identifying the values of the elastic constants in FE modelling at transverse impact, giving rise to the development of more accurate numerical models.

2 Ballistic experiments and FE model set-up

In order to identify one or more criteria for evaluating the results of ballistic behaviors of Dyneema® woven fabric model in the orthogonal experiments, ballistic experiments were carried out for a single Dyneema® woven fabric. Repeatable results would be taken as the criteria for the orthogonal experiments.

2.1 The fabric specimen and experimental set-up

The fabric specimen used in the present study is plain woven fabric with 175tex Dyneema® yarn. Its warp and weft densities are both 7 threads per centimeter. The areal density of the fabric is 252g/m^2. The thickness of the fabric is around 0.58mm, and the fabric specimens were cut into squares of 240×240mm.

The ballistic range used in this study consists of a shooting device, velocity detectors, fabric target panel, panel clamp, light sources and a high-velocity video camera, as described a previous paper [20]. By using this clamp, fabric specimens were clamped at 4 edges. The ballistic performance of specimens was evaluated using the energy loss of the projectile after

penetrating the panel, which is calculated from the impact velocity (V_i) and the residual velocity (V_r) of the projectile below:

$$\Delta \mathrm{E} = \frac{1}{2}\mathrm{m}(V_i^2 - V_r^2) \quad (1)$$

where m is the projectile mass. The projectile mass in this experiment is 1g and the length and diameter of the cylindrical projectile are both 5.5mm. Seven Dyneema® fabric specimens were prepared, each of which was tested once, and their mean value was taken. Owing to the tight clamp system, the yarn slippage was very small. The length of the yarn slippage at the edges was measured less than 1.0% of the whole length of the fabric specimen. The impact velocity of firing projectile is in the vicinity of 485m/s, and the high-velocity camera was used to record the ballistic event. The frame frequency was selected to be 180 KHz, which means the interval between two adjacent frames is 5.56μs.

2.2 Experimental results

From the experiments on the single layer of Dyneema® fabrics, the average value of energy absorption is 13.16J with a standard error of 0.44. The successive photographs taken from the back of the target panel during the ballistic event is demonstrated in Figure 2. In image (f), one vertical primary yarn (as pointed at) was stretched to straight whilst in image (h) it became curled, indicating the yarn was broken. Hence, it was reasonable to believe that the first yarn failure took place between 27.78μs and 38.89μs. In the repeated tests, the first yarns failure occurred during the same period.

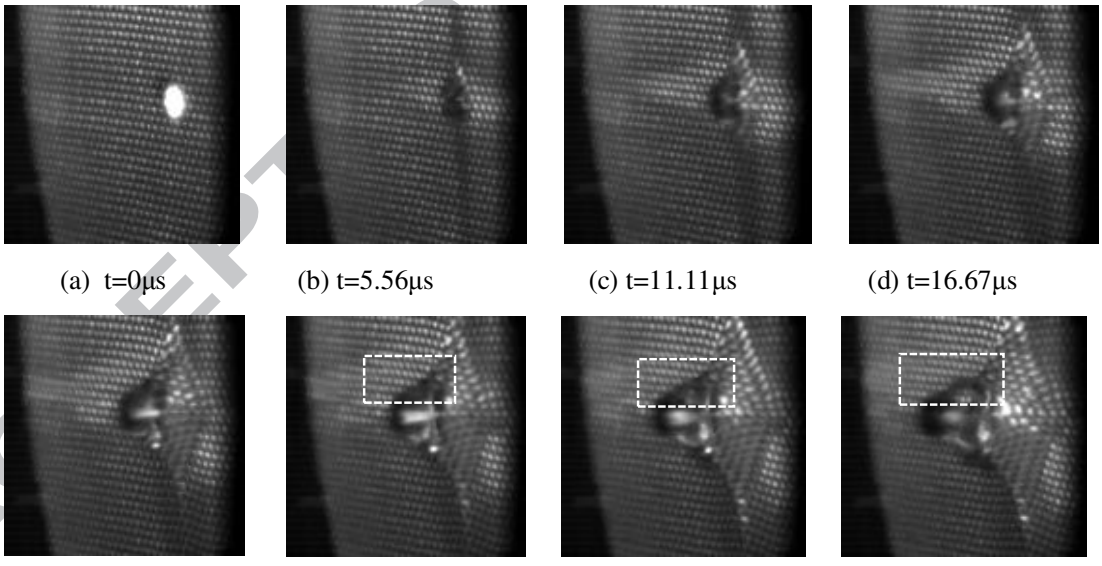

(a) t=0μs (b) t=5.56μs (c) t=11.11μs (d) t=16.67μs

(e) t=22.22μs (f) t=27.78μs (g) t=33.33μs (h) t=38.89μs

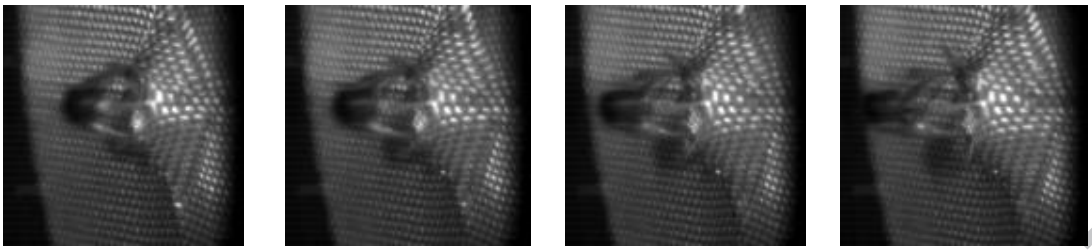

(i) t=44.44μs (j) t=50μs (k) t=55.56μs (l) t=61.11μs

Figure 2. Photographs of the single-layer Dyneema® fabric being penetrated by the projectile

Another performance index which can be obtained from the experiments is the number of failed yarns during the ballistic event. It is shown in Figure 3 that only two primary yarns completely failed after the fabric penetration. As a matter of factor, the number of failed yarns was shown to be either one or two in all the tests.

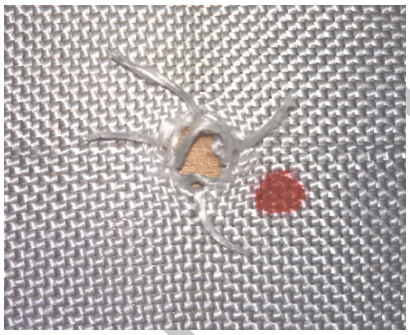

Figure 3. The configuration of the impacted fabric

The collective results on energy absorption, failure time of the first yarn broken, and number of failed yarns from the 7 ballistic tests are listed in Table 1.

Table 1. Collective results from the 7 ballistic tests

	Impact velocity (m/s)	Residual velocity (m/s)	Energy Absorption (J)	Time range of the first yarn failure (μs)	Number of failed yarns
1	474.75	449.13	11.83	27.78 ~38.89	1
2	519.34	495.21	12.24	27.78 ~38.89	2
3	491.12	460.56	14.54	27.78 ~38.89	2
4	478.62	450.81	12.92	27.78 ~38.89	1
5	437.21	401.78	14.86	27.78 ~38.89	2
6	491.63	465.89	12.32	27.78 ~38.89	2
7	492.15	464.10	13.41	27.78 ~38.89	2

2.3 Development of a FE model for the plain woven fabric

The plain woven fabric models for ballistic impact simulation were invariably created using the meso-scale yarn-level 3D orthotropic continuum model in a number of studies [21-26]. The individual yarns composed of solid elements were assembled to a woven fabric model for FE simulation. Nilakantan *et al.* [26] used this model to study the ballistic impact modelling of woven Kevlar® KM2 fabrics and obtained a significant validation in comparison

with the experimental results. Talebi *et al.* [27] studied the projectile nose angle effects on ballistic perforation of Twaron® fabric model using the yarn-level 3D orthotropic continuum model. A healthy agreement between FE simulation and experimental results was showed in this study. This model also was used by Wang *et al.* [10] who obtained a satisfactory validation in terms of the different impact and residual velocity of the projectile. Moreover, in these studies, the geometric model of the yarn and the fabric were developed based on the real ones, and so were the boundary conditions of the fabric and shapes of the rigid projectile models. Eight-node solid elements were used in these studies.

The FE model in this study was created on the basis of the same principle as the above models using ABAQUS® Explicit. The geometric model of the woven fabric was developed by combining the warp and weft yarn models. According to measurements, the cross-sectional shape of the yarn was assumed to be of the lenticular shape [28], consisting of two arcs facing opposite directions. The cross-sectional shape and area remained constant along the length of yarns for simplicity. Based on the measurement of the real fabric made of the Dyneema® yarn of 175tex with thread density of 7 threads/cm, the width and height of the warp and weft yarns were assumed identical to 1.20mm and 0.29mm for the dimension of the warp and weft yarns were measured very closely in reality as shown in Figure 4(a). Such assumptions appear to be reasonable for they were widely used in FE modelling of plain woven fabrics, with continuous filament yarns, subject to transverse impact, and the modelled results agreed well with the experimental results [29-32].

A circular woven fabric panel with diameter 240mm was constructed from 44 yarns with different lengths, and the simulation outcome was found no substantial differences (<3%) from using the 240×240mm square fabric model in terms of energy absorption and the failure time of the yarns. The thickness of the fabric model was 0.58mm, which is the same as the real fabric. The yarn cross-section was meshed using 10 first-order C3D8R solid elements and a full wave length of yarn contained 130 such elements. This type of element can provide good results at expense of the least computational effort [33, 34]. Default hourglass, distortion and element deletion were selected to prevent excessive distortion of elements and model instability [34, 35]. To obtain accurate results without consuming unnecessary resources, a mesh convergence study for mesh size along the yarn was also carried out. Convergence is obtained based on energy absorption and yarn failure time when a straight yarn model is under ballistic impact. The model with 10-mesh yarn cross-section used in this study demonstrated only less than 5% difference in energy absorption and yarn failure time than that with 18-mesh yarn cross-section, but a far more difference compared to coarser yarn meshing schemes – the difference in energy absorption was 92.3% and that for yarn failure time is 104% when compared to 6-mesh yarn cross section meshing scheme. Based on this analysis, the 10-mesh yarn cross-section scheme is considered to be adequate to ensure that mesh convergence is complete [36, 37]. The practical projectile was made from steel and it is in a cylindrical shape, and its model was developed as a rigid cylinder whose length and diameter were both 5.5mm. The projectile velocity in the FE simulation was chosen to be 500m/s following the practical test. The total time allowed for the impact process was set to be 55μs so as to catch all the information from the impact event. Assuming that the projectile

lands in the middle of fabric model, the projectile would contact 6 yarns (3 warp and 3 weft), and this is shown in Figure 4(b). The red circles present the outline of the chamfered cylindrical projectile.

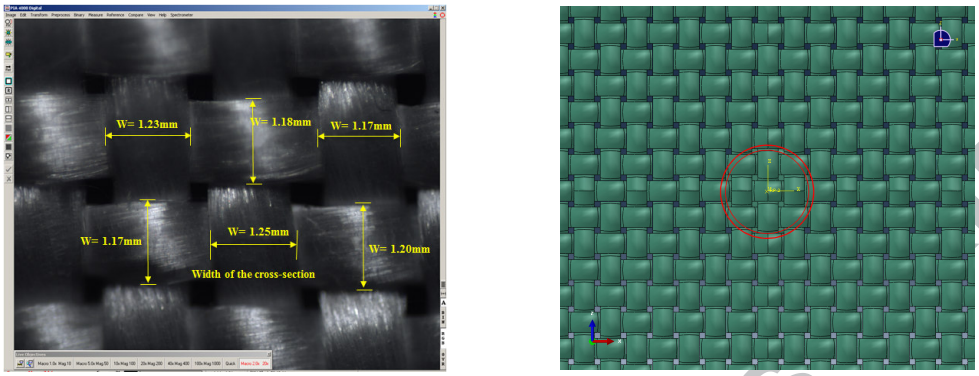

(a) Real fabric with measurement (b) Geometric model of the fabric

Figure 4. Real fabric and fabric model with impact position

3. Orthogonal experiments

3.1 Orthogonal array experimental designs

3.1.1 Introduce of the orthogonal array experimental designs

In the design of experiment, for various factors with different levels, the full factorial combinations are easily determined by calculating (number of levels)$^{\text{number of factors}}$. However, such a massive number of experiments are extremely difficult and time-consuming to be carried out. In order to identify the major effects in the experiments using only a fraction of possible combinations, orthogonal experiment was developed by based on the probability theory and mathematical statistics [38].

In designing an orthogonal array, several factors and their levels are first selected on the basis of the experience. A blank factor, sometimes, is created to obtain the influence of potential factors including factors excluded from the experiment, uncontrollable factors and possible experimental error [39, 40]. The levels of the blank factor, unlike the levels of other factors, can be defined to numbers or letters which have no substantial significance but are notations used to distinguish different levels of the potential factors for identifying the weight of potential factors, which indicates the health of the experimental design [40, 41]. After factors and levels are determined, an orthogonal array can be determined based on the work of Taguchi on a special set of orthogonal arrays for designing experiments with different numbers of factors and of levels [38]. According to the designed combinations, the experiments can be carried out. The results are analysed using a serial of mathematical calculations to obtain the weight of each factors and to optimise the experiments. Details will be provided in late sections.

3.1.2 Level selection for the factors

In creating the FE model, the plastic strength along the longitudinal direction was specified to 3.90GPa and its failure strain was to be 0.05 [42]. The transverse compression strengths were assigned to be 0.877GPa [43], and the shear strengths were assigned to be 0.58GPa [44]. Friction between the yarns and that between the projectile and the Dyneema® yarns were modelled by the hard contact-penalty algorithm provided in ABAQUS®. The friction coefficient was set to 0.05 [45] and applied for all contact situations for simplicity. For the Dyneema® yarn, the yarn-to-impactor frictional coefficient was commonly seen to be set from 0.01 to 0.17 [30][46][47] while the yarn-to-yarn friction coefficient was assigned to a value between 0.05 and 0.12 [30][45][47]. Moreover, according to studies from Chu [48], when the yarn-to-impactor and yarn-to-yarn frictional coefficients were lower than 0.2 their influence on the energy absorption of the Dyneema® woven fabric at the ballistic impact were not significant. Accordingly, the yarn-to-impactor and yarn-to-yarn frictional coefficients were assumed to be the same for this study and were not considered as one of the parameters.

Based on the real situation of untwisted multi-filament Dyneema yarns, E_{22} and G_{12} was assumed as the same to E_{33} and G_{13} respectively, and Poisson ratios ν_{12}, ν_{13} and ν_{23} were taken to be identical according to literature [6, 8, 9, 12, 15]. Hence, only five yarn elastic properties, namely E_{11}, E_{33}, ν, G_{13} and G_{23}, needed to be considered for elastic constants. According to the aforementioned studies for properties of UHMWPE yarns in longitudinal direction under high strain rate tests, the E_{11} was in the range from 80GPa to 130GPa. Cuniff [2] reported that the longitudinal stress dissipation speed of a yarn was dependent on the E_{11} and the volumetric density, which influenced the ballistic behaviour of the yarn or the yarn-made fabric. Chu *et al.* [49] numerically studied the influence of these two properties on the ballistic impact behaviour, and indicated that the influence of E_{11} was significant when it changed from 84GPa to 126GPa whereas the thread density of the fabric had little influence on the ballistic performance of the fabric. In the orthogonal experiment, E_{11} was considered as one factor with five levels, *viz.* 80GPa, 90GPa, 100GPa, 110GPa and 120GPa, to identify the weight of E_{11} in this range among five elastic constants. For other four elastic constants, previous studies indicated that they also had significantly influence on the tensile and transverse behaviour of the fabric [13-15, 19, 37]. Therefore, E_{33}, ν, G_{13} and G_{23} were taken as the other four factors. For the isotropic model, the values of E_{33}, G_{13} and G_{23} were determined by the value of E_{11} and ν and they cannot be considered independently. Hence, the values of E_{33}, G_{13} and G_{23} used in isotropic model were not considered in this study as the levels for the factors. The selection of the levels of these four factors was based on the previous studies for UHMWPE yarn or similar material yarns and the levels chosen in present study covered all the levels of each factor of UHMWPE yarn in the previous studies in Table 2. The levels of Poisson ratio ν was chosen from 0 to 0.4 with an even interval of 0.1. The values of E_{33}, G_{13} and G_{23} were picked from 0.37GPa to 6GPa, with the interval between sequent levels twice smaller than the former level to cover wider range with fewer levels. Table 2 shows five factors of elastic constants for the UHMWPE yarn, each with five levels.

In addition, an extra factor called blank was created to record the influence of other potential factors. This factor also has five levels in parallel to the other factors. In this particular study unlike the practical experiments, the simulation conditions can be fixed in each trial, thereby leading to thorough repeatability of each trial [50]. Moreover, except for these five factors,

other influential factors were fixed with solid evidence. Thus, the blank column was deduced to represent the interaction between these factors.

Table 2. Levels and factors of elastic constants of Dyneema® yarn

Levels	E_{11}(GPa)	E_{33}(GPa)	ν	G_{13}(GPa)	G_{23}(GPa)
1	120.00[5][6]	6.00[6]	0.00[9]	6.00[6]	6.00[6]
2	110.00[7]	3.00[30]	0.10	3.00[8]	3.00
3	100.00	1.50[11]	0.20[8]	1.50	1.50
4	90.00[4]	0.75[51]	0.30[6]	0.75[9][52]	0.75[52]
5	80.00[3]	0.37[53]	0.40	0.37	0.37

3.1.3 Design of orthogonal array

For the factors and levels in this study, an orthogonal table L_{25} (5^6) in Table 3 was created based on [38][41]. The notation L is for Latin squares while the subscript refers to the number of rows in the table and indicates the number of combinations. In this table, six factors were represented by A, B, C, D, E and X. Twenty-five trials were carried out according to the L_{25} matrix to complete the optimization process. Each row of the table represents a run and is a specific group of levels to be simulated. The run order was random to avoid subjective bias [40]. It took approximately 6 hours for each trial by using a computer with Core i5-3470 3.2GHz CPU and 24GB RAM. In order to evaluate each group of combination, energy absorption, failure time of the first yarn broken and the number of failed yarns were obtained in the FE simulation. These three performance indices were chosen for they are easy to obtain through experiments and simulation, and they reflect the nature of ballistic failure of the fabrics. After obtaining these results from the orthogonal experimental trials, data analysis was carried out using the range analysis and analysis of variance (ANOVA).

Table 3. Impact results in OA_{25} matrix

	Factors						**Results**		
Group No.	A E_{11} (GPa)	B E_{33} (GPa)	C ν	D G_{13} (GPa)	E G_{23} (GPa)	X Blank	Energy Absorption (J)	Time of the first failed yarn (μs)	Number of failed yarns
1	120.00	1.50	0.10	0.75	1.50	2	9.52	7.00	4
2	80.00	1.50	0.40	6.00	0.37	4	4.05	2.00	6
3	120.00	6.00	0.00	6.00	6.00	1	2.62	2.00	6
4	110.00	0.37	0.40	0.37	1.50	1	16.70	39.00	2
5	120.00	0.75	0.40	1.50	0.75	5	2.94	1.00	6
6	90.00	1.50	0.20	1.50	3.00	1	7.65	6.00	6

7	80.00	0.75	0.20	0.37	6.00	2	1.89	1.00	6
8	90.00	6.00	0.10	0.37	0.37	5	12.07	22.00	2
9	110.00	1.50	0.30	3.00	6.00	5	2.85	2.00	6
10	100.00	0.37	0.10	1.50	6.00	4	2.29	1.00	6
11	100.00	1.50	0.00	0.37	0.75	3	14.29	10.00	4
12	120.00	0.37	0.20	3.00	0.37	3	2.32	1.00	6
13	90.00	0.37	0.30	6.00	0.75	2	2.27	2.00	6
14	80.00	0.37	0.00	0.75	3.00	5	9.90	6.00	6
15	80.00	3.00	0.10	3.00	0.75	1	5.53	1.00	6
16	90.00	3.00	0.40	0.75	6.00	3	2.19	1.00	6
17	110.00	3.00	0.00	1.50	0.37	2	5.44	2.00	6
18	80.00	6.00	0.30	1.50	1.50	3	4.55	3.00	6
19	100.00	0.75	0.30	0.75	0.37	1	12.35	12.00	4
20	120.00	3.00	0.30	0.37	3.00	4	4.26	3.00	4
21	90.00	0.75	0.00	3.00	1.50	4	3.16	2.00	6
22	100.00	3.00	0.20	6.00	1.50	5	3.18	2.00	6
23	100.00	6.00	0.40	3.00	3.00	2	3.48	2.00	6
24	110.00	6.00	0.20	0.75	0.75	4	13.00	1.00	4
25	110.00	0.75	0.10	6.00	3.00	3	2.36	1.00	6

3.2 Range Analysis

Range analysis leads to observations and conclusions in the following three areas: (i) factor influence or main effects, (ii) optimum condition for desired quality characteristics, and (iii) performance expected at the optimum condition [54]. A range analysis includes two critical parameters K_{ji} and R_j. K_{ji} is the sum of the evaluation index of level i for factor j and its mean value $\overline{K}_{ji}$ determines the optimal combination, whereas R_j is the range between the maximum and minimum values of the mean value $\overline{K}_{ji}$ of K_{ji} and it is used to evaluate the weight of the factors. The larger is R_j of a factor, the more significant is the factor [55]. The equations for calculating $\overline{K}_{ji}$ and R_j are shown below [40]:

$$\overline{K}_{ji} = \frac{1}{N_i}\sum_{j=1}^{N_i} y_{ji} \quad (2)$$

$$R_j = \max\left(\overline{K}_{j1}, \overline{K}_{j2}, \ldots, \overline{K}_{ji}\right) - \min\left(\overline{K}_{j1}, \overline{K}_{j2}, \ldots, \overline{K}_{ji}\right) \quad (3)$$

where i is the level number (in this study i = 1, 2, 3, 4, or 5), j is factor notation (A, B, C, D, E or X in this study), y_{ji} is one result value for factor j at level i, and N_i is the total number of levels [40].

3.3 Analysis of variance (ANOVA)

3.3.1 F value and P value

The range analysis can identify the order of factors in terms of their influence, but the extent to which each factor can influence the performance results as well as its confidence level needs to be specified. ANOVA is a standard statistical technique used to determine the extent of influence, to estimate the confidence level of the influence and to evaluate the experimental errors [40, 54]. For doing these, F and P values of the factors are used. An F value of each factor represents the ratio of the sum of the square of each factor's average deviations to that of the experimental error [40]. The calculation of the F value demands the sum of square deviation for each factor (SS_j), the total sum of the squared deviation (SS_T), the degree of freedom of the factor j (df_j) and the total degree of freedom of the experiments (df_T). df_j is equal to the number of levels of factor j minus 1 while df_T the total number of experiments m minus 1. Thus, the degree of freedom of the experimental error df_e is the difference between df_T and the sum of the df_j of all the factors.

SS_j of the factor j and SS_T are calculated using the following equations [40]:

$$SS_j = \frac{1}{n}\sum_{i=1}^{n} K_{ji}^2 - \frac{\left(\sum_{i=1}^{n^2} Y_i\right)^2}{n^2} \quad (4)$$

$$SS_T = \sum_{i=1}^{m} Y_i^2 - \frac{1}{m}\left(\sum_{i=1}^{m} Y_i\right)^2 \quad (5)$$

where n is the number of levels of factor j and Y_i is the value of the result of the level i [40].

Accordingly, the sum of square deviation for error (SS_e) is calculated by SS_T subtracting the sum of SS_j [56]. Variance for factor j (V_j) and variance for experimental error (V_e) are expressed below:

$$V_j = \frac{SS_j}{df_j} \quad (6)$$

$$V_e = \frac{SS_e}{df_e} \quad (7)$$

The F value for each factor (F_j) is defined as

$$F_j = \frac{V_j}{V_e} \quad (8)$$

Factor j has a significant effect only when $F_j > 2$ [40].

The purified sum of the squared deviation for factor j (SS'_j) is defined by Equation 9, and the percent contribution of factor j (P_j) and the percent contribution of experimental error (P_e) are calculated using Equations 10 and 11 respectively.

$$SS'_j = SS_j - V_e \times df_j \quad (9)$$

$$P_j = \frac{SS'_j}{SS_T} \times 100\% \quad (10)$$

$$P_e = \frac{SS'_e}{SS_T} \times 100\% \quad (11)$$

Low percentage of experimental error indicates that no important factors were omitted in the orthogonal design, but high percentage of experimental error does not mean the orthogonal experiment is unreliable even if it is higher than 50% [57]. The high percentage of experimental error attributes to experimental error, factors not included in the experiment, and uncontrollable factors. For the case of high percentage of experimental error, the reason should be identified [57].

3.3.2 Pooling technique

In some cases, df_e is 0, which causes V_e to be indeterminate. Although the P_j and P_e values can be worked out providing evidence for significance of the factors, the F value for each factor will not be able to be calculated. In such a circumstance, the pooling technique is used.

The pooling technique ignores one or more factors considered insignificant as if they were not present and ANOVA results are revised and re-estimated. In the case of df_e=0, two types of mistakes would always be encountered statistically. The first one takes something as important when it is not, and another is the ignorance of significant factors [39]. The polling technique is used to minimize the chance of the first mistake, and in this particular study, the second mistake can be excluded since other factors in the FE simulation can be fully controlled and the FE modelling can be well repeated. The selection of a pooled factor starts with the factor of the least influence in terms of the *SS* value following the rule of polling the factor whose influence is less than 10% of the most influential factor [57]. After polling the factor, the F value and purified sums can be recalculated by using Equations 6, 7, 8 and 9.

4. Results and discussion

4.1 Energy Absorption and statistical analysis

4.1.1 Range analysis

According to the Equations 2 and 3, the analysis results for energy absorption of single layer Dyneema® fabric models are demonstrated in Table 4 and Figure 5. As can be seen from Figure 5, the factor effect as represented by R_j on the energy absorption is in the order of the following: Factor D (G_{13}) > Factor E (G_{23}) > Factor X (Interactions) > Factor A (E_{11}) > Factor B (E_{33}) > Factor C (ν). G_{13} is found to be of the most importance to determine the energy absorption of this single layer Dyneema® fabric model whereas Poisson's ratio is the least.

Table 4. Range analysis of energy absorption

	j / *i*	A	B	C	D	E	X
$\overline{K}_{ji}$	1	4.33	7.14	7.08	2.90	2.37	8.97
	2	8.07	4.12	6.35	3.47	5.53	4.52
	3	7.12	7.67	5.61	4.57	7.42	5.14
	4	5.47	4.54	5.25	9.39	7.61	5.35
	5	5.18	6.70	5.87	9.84	7.25	6.19
R_j		3.74	3.55	1.83	6.94	5.24	4.45

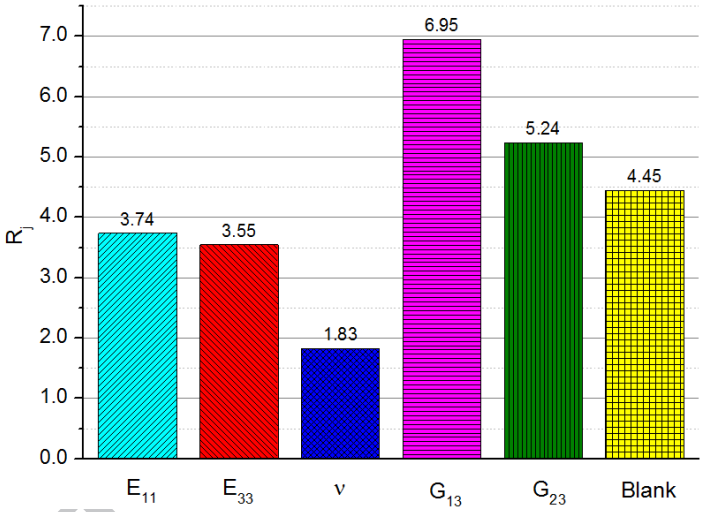

Figure 5. Range values of different factors in the energy absorption

Figure 6 illustrates relationship between the mean values $\overline{K}_{ji}$ of each factor (energy absorption) and the levels of the real factors. These graphs show the influence of each factor on energy absorption of the modelled panel. Such relationships provide useful information for further analysis and discussion. As can be seen from Figure 6(a), the increase of E_{11} is sensitive to cause increase of energy absorption between 80GPa and 110GPa with the lowest sensitivity between 80GPa and 90GPa, and sensitive to cause sharp decrease in energy absorption between 110GPa and 120GPa. The influence of E_{33} does not seem to have a stable pattern as shown in Figure 6(b), indicating a lower significance of E_{33} in determining the ballistic performance of the model. Increase in material Poisson's ratio ν from 0 to 0.3 is quite sensitive for an almost linear decrease in energy absorption, and further increase in the Poisson's ratio will cause the energy absorption to increase, which is evident in Figure 6(c). However, it should be noted that influence on energy absorption is the smallest as shown in both Figure 5 and Figure 6(c). Sharp decreases of energy absorption are witnessed in Figure 6(d) as G_{13} is increased from 0.37GPa to 3.00GPa, and then the sensitivity is much reduced from G_{13} = 3.00GPa to 6.00GPa. Figure 6(e) shows that the first 3 levels of values of G_{23} do

not demonstrate sensitive influence on the energy absorption, but from G_{23} = 1.50GPa to 6.00GPa the energy absorption decreases linearly with a notable sensitivity.

The maximum value of energy absorption associated to considered levels of the factors is closer to the values obtained from the corresponding experimental results, and such level values, i.e. $A_2B_3C_1D_5E_4$, are used for simulation in the first place, where A, B, C, D and E indicate the five factors and their subscripts are the level number.

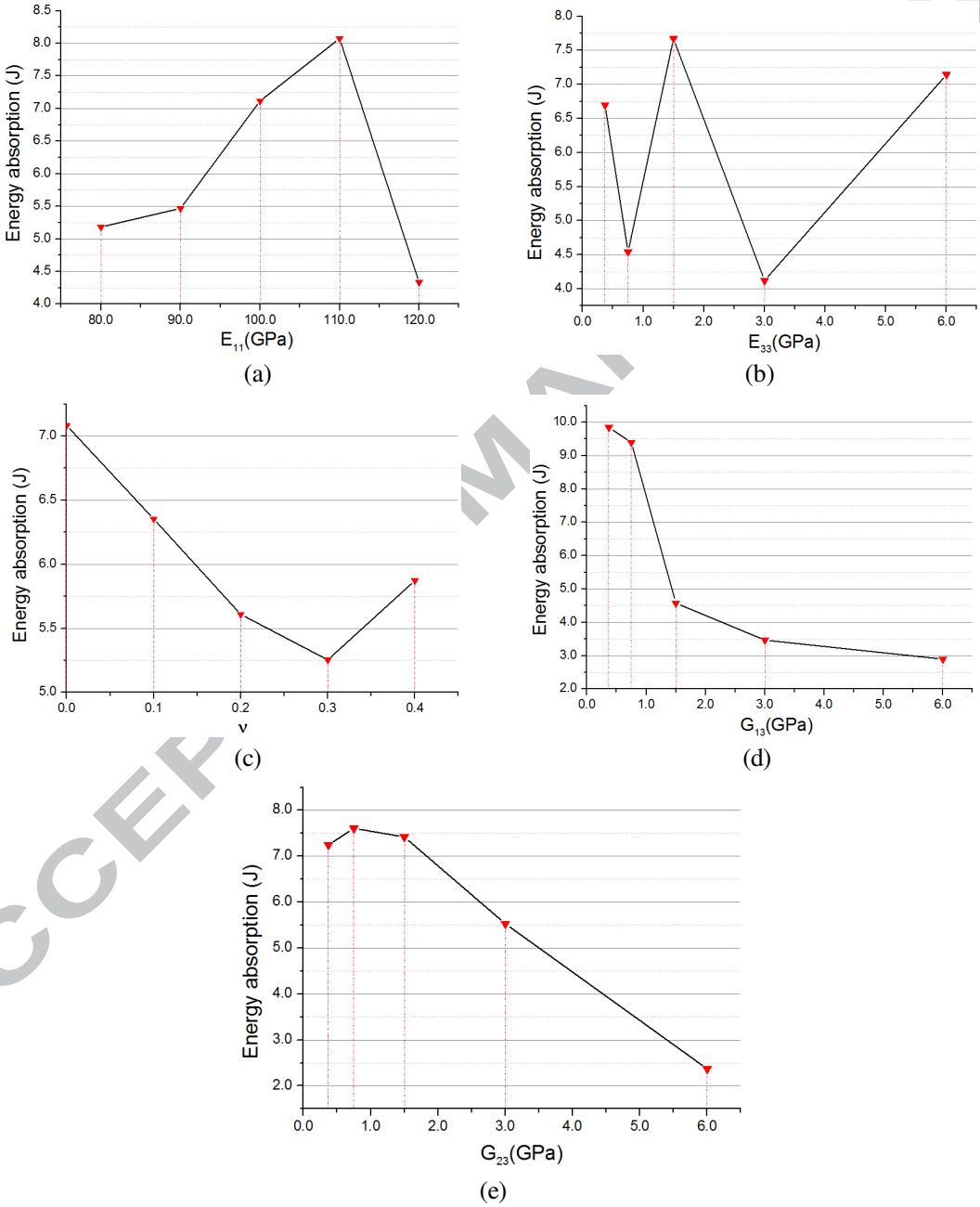

Figure 6. Relationship between factor levels and energy absorption: (a) E_{11}; (b) E_{33}; (c) ν; (d) G_{13}; (e) G_{23}.

4.1.2 Analysis of variance

The ANOVA results for the energy absorption before pooling are listed in Table 5. In this study, *df* of experimental error is equal to zero. Therefore, *F* and *P* values for the error could not be calculated and nor was the *F* value of factors. However, according to this table, the relative influence of each factor concerning the percent contribution to the overall response can be specifically identified. Factor D (G_{13}) is the most influential factor accounting for 45.42% of the overall response among the six while Factor C (ν) is the least only accounting for 2.07%. The dominance of the G_{13} is obvious with the *P* value more than twice than that of the second influential factor G_{23}. Factor X (interactions) is relatively low at 12.51% but not completely negligible, indicating that there exist some influences of the interactions between two or more factors.

Table 5. ANOVA results of the energy absorption

Source	*SS*	*df*	*V*	*F*	*SS'*	*P* (%)
A (E_{11})	46.35	4	11.59	--	46.35	9.49
B (E_{33})	51.19	4	12.80	--	51.19	10.49
C (ν)	10.09	4	2.52	--	10.09	2.07
D (G_{13})	221.75	4	55.44	--	221.75	45.42
E (G_{23})	97.76	4	24.44	--	97.76	20.02
X (interactions)	61.09	4	15.27	--	61.09	12.51
e	0	0	--	--	--	--
T	488.23	24			488.23	100

Note: SS - the sum of square deviation; df - the degree of freedom; V - the variance; F - F value; SS' - the purified sum of square deviation; P - the percent contribution.

Table 6 demonstrates the ANOVA results for the energy absorption after pooling. The least influential Factor C (*v*) is pooled and the F value of each factor is calculated. The F value is compared to the value of $F_{\alpha}(a, b)$ which indicates the threshold *F* value with the risk level α (confidence level = 1- α), where *a* and *b* are the degrees of freedom associated to the numerator and denominator respectively. In this study, the degrees of freedom associated to numerator and denominator are both 4. Therefore, $F_{\alpha}(4, 4)$ can be found in the distribution table of the *F* value. For $\alpha = 0.01$, $F_{0.01}(4, 4)=16.00$, and for $\alpha = 0.05$, $F_{0.05}(4, 4) = 6.39$ [58]. The *F* value of Factor D (G_{13}) is 21.98 which is larger than $F_{0.01}(4, 4)$, indicating that the result is at the confidence level of 99%. Similarly, the *F* value of Factor E (G_{23}) equates to 9.69, larger than $F_{0.05}(4, 4)$ but smaller than $F_{0.01}(4, 4)$, hence with a confidence level of 95%. These re-estimated results manifest that Factor C (*v*) is relatively insignificant to the energy absorption. The recalculated percent contribution shows that the absence of *v* leads to the 12.40% experimental error. According to the percent contribution, it could be speculated that the most significant factor in terms of the energy absorption was Factor D (G_{13}) with a *P* value of 43.35%, followed by Factor E (G_{23}) with a *P* value of 17.96%. The *P* values of the other three factors are around 10%.

Table 6. ANOVA results of the energy absorption after pooling

Source	*SS*	*df*	*V*	*F*		*SS'*	*P(%)*
A (E_{11})	46.35	4	11.59	4.60	--	36.27	7.42
B (E_{33})	51.19	4	12.80	5.08	--	41.10	8.42
C (ν)	(10.09)	(4)	--	pooled	--	--	--
D (G_{13})	221.75	4	55.44	21.98	$> F_{0.01}(4,4)$	211.66	43.35
E (G_{23})	97.76	4	24.44	9.69	$> F_{0.05}(4,4)$	87.67	17.96
X (interactions)	61.09	4	15.27	6.06	--	61.09	10.45
e	10.09	4	2.52	--	--	--	12.40
T	488.23	24				488.23	100

4.2 Time of the first yarn failure and statistical analysis

4.2.1 Range analysis

On the basis of the Equation 2 and 3, the range analysis results for the failure time of the first broken yarn in single layer Dyneema® fabric models at high speed impact are demonstrated in Table 7 and Figure 7. The factor effect on the time of the first failed yarn is determined in the order as follows: Factor D (G_{13}) > Factor E (G_{23}) = Factor X (Interactions) = Factor A (E_{11}) > Factor B (E_{33}) > Factor C (ν). According to this result, the G_{13} also behaves as the most important factor while ν as the least.

Table 7. Range analysis of time of the first broken yarn

	j / ***i***	**A**	**B**	**C**	**D**	**E**	**X**
$\bar{K}_{ji}$	1	2.80×10^{-6}	7.80×10^{-6}	4.40×10^{-6}	1.80×10^{-6}	1.40×10^{-6}	1.20×10^{-5}
	2	1.08×10^{-5}	1.80×10^{-6}	6.40×10^{-6}	1.60×10^{-6}	3.60×10^{-6}	2.80×10^{-6}
	3	5.40×10^{-6}	5.40×10^{-6}	4.00×10^{-6}	2.60×10^{-6}	1.06×10^{-5}	3.20×10^{-6}
	4	6.60×10^{-6}	3.40×10^{-6}	4.40×10^{-6}	7.20×10^{-6}	4.80×10^{-6}	3.60×10^{-6}
	5	2.60×10^{-6}	9.80×10^{-6}	9.00×10^{-6}	1.50×10^{-5}	7.80×10^{-6}	6.60×10^{-6}
$\mathbf{R}_j$		8.20×10^{-6}	8.00×10^{-6}	5.00×10^{-6}	1.34×10^{-5}	9.20×10^{-6}	9.20×10^{-6}

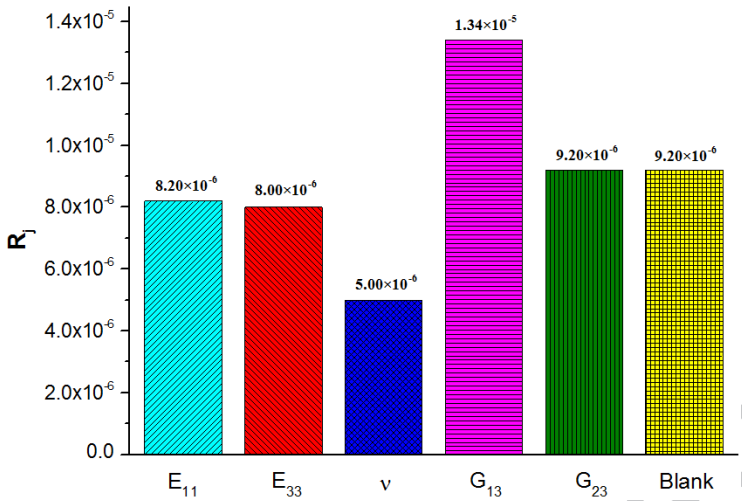

Figure 7. Range values of different factors in the failure time of the first yarn broken

The relationship between mean values $\overline{K}_{ji}$ of each factor and failure time of the first yarn broken are demonstrated in Figure 8(a)-(e). As shown in Figure 8(a), increasing E_{11} results in variation in yarn failure time, with the peak value at E_{11} = 110GPa. The sharp decrease in yarn failure time coincides with the energy absorption caused by changing E_{11} as indicated in Figure 6(a). The shape of the curve indicating the influence of G_{13} on the yarn failure time shown Figure 8(d) is similar to that of influence of G_{13} on the energy absorption, and this curve suggests that the yarn failure time is sensitive when G_{13} alters from 0.37GPa to 1.50GPa. Moreover, the lower value of G_{13} could facilitate extension of the active time of the yarns, thereby increasing the energy absorption of the fabric. The use of such G_{13} values makes the modelled results closer to the experimental results. Figure 8(e) demonstrates the influence of G_{23} on the yarn failure time in FE calculation. When it is higher than 1.50GPa, the yarn failure time monotonically decreases, implying notable sensitivity of yarn failure time to the G_{23} in the range from 1.50GPa to 3.00GPa. The influences of E_{33} and ν on yarn failure time are illustrated in Figure 8(b) and (c) respectively.

In addition, the first yarn failure takes the longest time of 6.60μs, 9.8μs, 9μs, 15μs and 10.6μs when the E_{11}, E_{33}, ν, G_{13} and G_{23} are equal to 110GPa, 0.37GPa, 0.4, 0.37GPa and 1.50GPa respectively. When the time of the first yarn broken was the maximum value, it is closer to the time range of the first yarn broken from the experiments. Therefore, these levels are chosen as the optimal options for the combination which could be deduced as $A_2B_5C_1D_5E_3$.

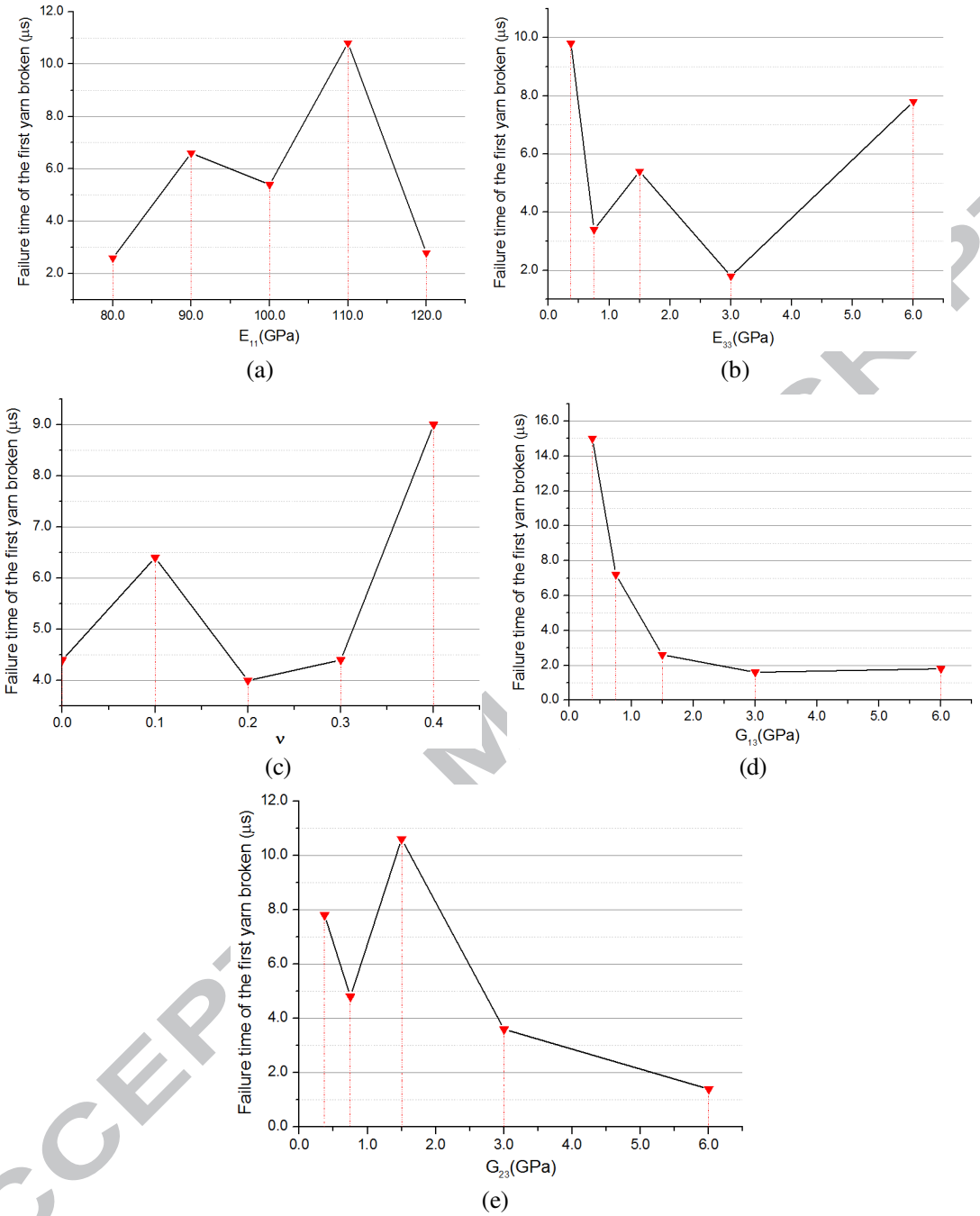

Figure 8. Relationship between factor levels and failure time of the first yarn broken: (a) E_{11}; (b) E_{33}; (c) ν; (d) G_{13}; (e) G_{23}.

4.2.2 Analysis of variance

Table 8 demonstrates the ANOVA results for the failure time of the first yarn broken before pooling. According to their *P* value, their relative percent influence on the failure time of the first yarn broken is in the order: Factor D (G_{13}) > Factor X (interactions) > Factor E (G_{23}) > Factor A (E_{11}) > Factor B (E_{33}) > Factor C (ν). G_{13} maintains its dominance with the percent

influence of 37.60% which is more than twice as important as that of the second influential factor. Factor C (ν) is pooled for its inconsiderable influence.

Table 8. ANOVA results of the failure time of the first yarn broken

Source	*SS*	*df*	*V*	*F*	*SS'*	*P (%)*
A (E_{11})	2.25×10^{-10}	4	5.61×10^{-11}	--	2.25×10^{-10}	13.00
B (E_{33})	2.09×10^{-10}	4	5.22×10^{-11}	--	2.09×10^{-10}	12.10
C (ν)	8.82×10^{-11}	4	2.20×10^{-11}	--	8.82×10^{-11}	5.09
D (G_{13})	6.50×10^{-10}	4	1.60×10^{-10}	--	6.50×10^{-10}	37.60
E (G_{23})	2.61×10^{-10}	4	6.51×10^{-11}	--	2.61×10^{-10}	15.00
X (interactions)	3.00×10^{-10}	4	7.40×10^{-11}	--	3.00×10^{-10}	17.20
e	0	0	--	--	--	--
T	1.73×10^{-9}	24			1.73×10^{-9}	100

The ANOVA results for the the failure time of the first yarn broken after pooling is shown in Table 9. It is obvious that only the *F* value for Factor D (G_{13}) was larger than $F_{0.05}(4, 4)$, which indicates that the G_{13} is the most significant factor in terms of the failure time of the first yarn broken when the result is at the confidence level of 95% even if Factor C (ν) is absent.

Table 9. ANOVA results of the failure time of the first yarn broken after pooling

Source	*SS*	d_f	*V*	*F*		*SS'*	*P (%)*
A (E_{11})	2.25×10^{-10}	4	5.61×10^{-11}	2.55		1.36×10^{-10}	7.88
B (E_{33})	2.09×10^{-10}	4	5.22×10^{-11}	2.37		1.21×10^{-10}	6.98
C (ν)	(8.82×10^{-11})	(4)	--	pooled		--	--
D (G_{13})	6.50×10^{-10}	4	1.60×10^{-10}	7.39	$> F_{0.05}(4,4)$	5.64×10^{-10}	32.55
E (G_{23})	2.61×10^{-10}	4	6.51×10^{-11}	2.96		1.73×10^{-10}	9.96
X (interactions)	3.00×10^{-10}	4	7.40×10^{-11}	3.38		2.10×10^{-10}	12.10
e	8.82×10^{-11}	4	2.20×10^{-11}	--		--	30.50
T	1.73×10^{-9}	24				1.73×10^{-9}	100

4.3 Number of failed yarns and statistical analysis

4.3.1 Range analysis

The analysis results for the number of broken yarn in single layer Dyneema® fabric models at high speed impact are illustrated in Table 10 and Figure 9. According to the comparison among R values in Figure 9, the weight of factors in terms of the amount of broken yarn is arranged in the sequences that: Factor D (G_{13}) > Factor E (G_{23}) = Factor A (E_{11}) = Factor X (Interactions) = Factor B (E_{33}) = Factor C (ν). It is shown that in terms of the amount of broken yarn, G_{13} is the most influential factor.

Table 10. Range analysis of the amount of broken yarns

	j / *i*	A	B	C	D	E	X
$\overline{K}_{ji}$	1	5.20	4.80	5.60	6.00	6.00	4.80
	2	4.80	5.60	4.80	6.00	5.60	5.60
	3	5.20	5.20	5.60	6.00	4.80	5.60
	4	5.20	5.60	5.20	4.80	5.20	5.20
	5	6.00	5.20	5.20	3.60	4.80	5.20
R_j		1.20	0.80	0.80	2.40	1.20	0.80

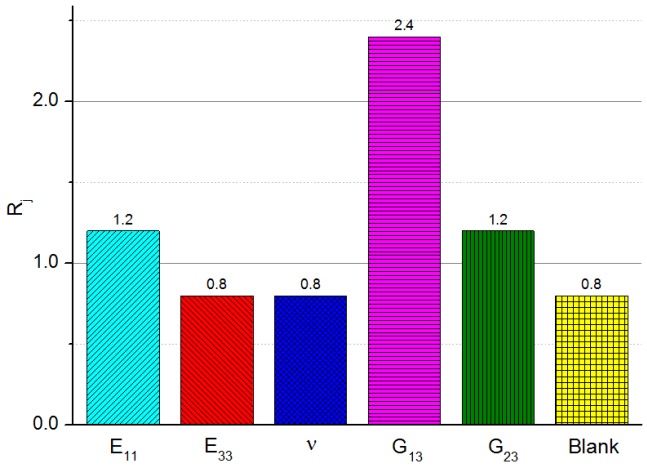

Figure 9. Range values of different factors in the amount of broken yarn

Figure 10 demonstrates the relationship between mean values $\overline{K}_{ji}$ of each factor and the number of failed yarns. Figure 10(a) shows that the increase in E_{11} causes an overall decrease of the number of yarns broken until E_{11} reaches 110GPa followed by an increase when E_{11} increases to 120GPa. The highest number of yarn failure occurs when E_{11} assumes its lowest level 80GPa. Whilst the influences of E_{33} and ν are not clear enough as shown in Figure 10(b) and (c), the increases in G_{13} and G_{23} tend to lead to higher numbers of yarn broken as illustrate in Figure 10(d) and (e).

In addition, the minimum values of the levels for Factor A, B, C and E are all equal to 4.8 when E_{11}, E_{33}, ν and G_{23} equate to 110.00GPa, 6.00GPa, 0.10 and 0.37GPa or 1.50GPa. For G_{13}, the minimum value of the level is 3.6 at 0.37GPa. In this result analysis, the minimum value of the level is closer to the experimental results. It is selected as the optimal value for the combination which could be speculated as $A_2B_1C_2D_5E_{3(5)}$.

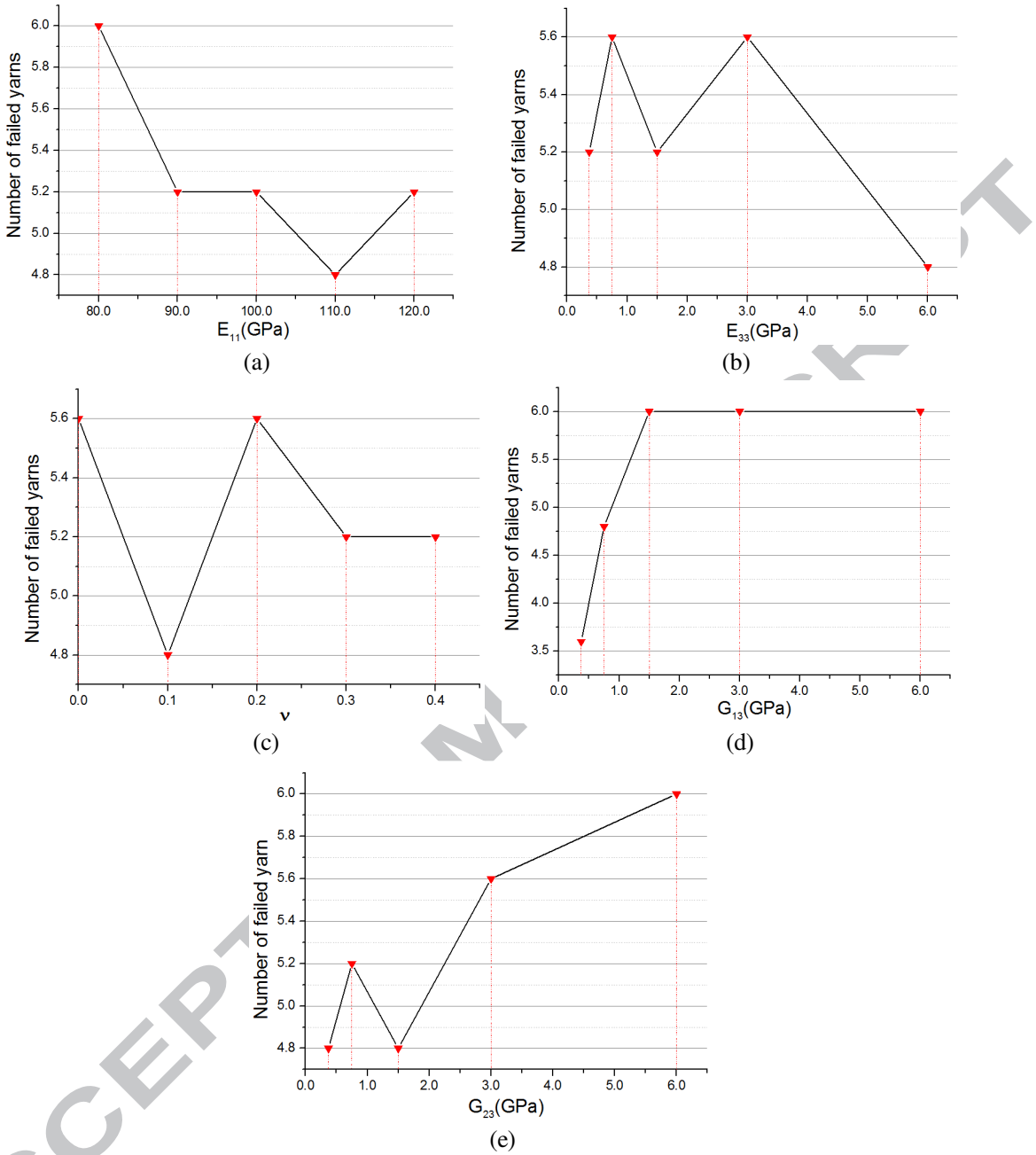

Figure 10. Relationship between factor levels and the number of failed yarns: (a) E_{11}; (b) E_{33}; (c) ν; (d) G_{13}; (e) G_{23}.

4.3.2 Analysis of variance

The ANOVA results for the number of failed yarns before pooling is illustrated in Table 11. The relative percent influence of Factor D (G_{13}, 59.00%) on the number of failed yarns is the most influential, followed by Factor E (G_{23}, 13.90%) and Factor A (E_{11}, 9.84%). Moreover, Factor B (E_{33}, 5.74%), Factor C (ν, 5.74%) and Factor X (interactions, 5.74%) are identical as the least significant factors. Thus, these three factors are pooled. However, the results of three of them pooled are the same as those of only one of them pooled.

Table 11. ANOVA results of number of failed yarns

Source	*SS*	*df*	*V*	*F*	*SS'*	*P (%)*
A (E_{11})	3.84	4	0.96	--	3.84	9.84
B (E_{33})	2.24	4	0.56	--	2.24	5.74
C (ν)	2.24	4	0.56	--	2.24	5.74
D (G_{13})	23.04	4	5.76	--	23.04	59.00
E (G_{23})	5.44	4	1.36	--	5.44	13.90
X (interactions)	2.24	4	0.56	--	2.24	5.74
e	0	0	--	--	--	--
T	39.00	24			39.00	100

After pooling, the ANOVA results for the number of failed yarns alter as shown in the Table 12. *F* value of Factor D (G_{13}) was higher than the value of $F_{0.05}(4, 4)$. This indicates that G_{13} is the most indispensable factor in terms of the number of failed yarns when the regression curve and analysis are with a confidence level of 95%. The *F* values and *P* values of these factors demonstrate the overwhelming dominant influence of G_{13} on the number of failed yarns when Factor B, C and X are absent.

Table 12. ANOVA results of number of failed yarns after pooling

Source	*SS*	*df*	*V*	*F*		*SS'*	*P (%)*
A (E_{11})	3.84	4	0.96	1.71		1.60	4.10
B (E_{33})	(2.24)	(4)	--	pooled		--	--
C (ν)	(2.24)	(4)	--	pooled		--	--
D (G_{13})	23.04	4	5.76	10.30	> $F_{0.05}(4,4)$	20.80	53.30
E (G_{23})	5.44	4	1.36	2.43		3.20	8.20
X (interactions)	(2.24)	(4)	--	pooled		--	--
e	6.72	12	0.56	--		--	34.40
T	39.00	24				39.00	100

4.4 Optimization of the combination of elastic constants

Due to the difficulties of measuring the transverse moduli, shear moduli and Poisson's ratio of continuous filament yarns and the requirements for development of an appropriate model with more accurate elastic constants, the optimization method was carried out to identify a combination of the elastic constant values in present study, whose results were matched with experimental ones.

According to the optimization results for each criterion (energy absorption: $A_2B_3C_1D_5E_4$; failure time of the first yarn broken: $A_2B_5C_1D_5E_3$; number of failed yarns: $A_2B_1C_2D_5E_{3(5)}$, the optimised one for Factor D (G_{13}) in terms of the three aspects all directed to level 5 (0.37GPa). Similarly, the optimal option for E_{11} was 110GPa. For Factor E (G_{23}) and Factor

C (ν), one level appeared twice in the optimum combinations concerning the three criteria. Thus, 1.50GPa was selected for G_{23} while 0 was selected for ν. Due to the relative insignificance of Factor B (E_{33}), the optimal option was chosen from either level in the three combinations. Therefore, the optimal selection of E_{11}, E_{33}, ν, G_{13} and G_{23} were 110GPa, 0.37GPa, 0, 0.37GPa, and 1.50GPa respectively. The whole combination was $A_2B_5C_1D_5E_3$.

However, the energy absorption of this combination was 18.84J which was much higher than the experimental results in Table 13. Similarly, the failure time of the first yarn broken was at 49μs, much higher than the time range from experimental work while the number of failed yarns was only one. This was due to the assumptions of taking maximum value as the optimum for energy absorption and failure time of the first yarn broken while taking minimum value as the optimum for the number of failed yarns. But the results from the combination of the elastic constants were excessively better than their counterparts from the 25 groups in Table 3. This verified the feasibility of the orthogonal experiment for identifying a better combination of elastic constants in terms of the ballistic performance of the Dyneema® woven fabric model.

In order to make the modelling results closer to the corresponding experimental ones, some adjustments of the elastic constants were made according to their result tendencies in Figure 6, Figure 8 and Figure 10. Factor D (G_{13}) should be fixed to 0.37GPa for its dominant influence. Due to the insignificance of Factor B (E_{33}) and Factor C (ν) regrading to the three criteria, they were not considered to be changed. As the second influential factor among the five, G_{23} was adjusted to next inferior level 0.37GPa in terms of the three criteria with fixed E_{11}. A new combination was created as $A_2B_5C_1D_5E_5$, whose results were still higher but closer to the experimental ones regarding energy absorption and failure time of the first yarn broken in Table 13. Furthermore, the E_{11} was then adjusted to 90GPa for more decrease of energy absorption on the basis of the tendency in the Figure 6 (a), which developed a combination of $A_4B_5C_1D_5E_5$. The energy absorption decreased to 16.26J but there was no yarn broken in this combination. In order to increase the number of failed yarns, G_{23} was selected to 0.75GPa based on the tendency in Figure 10 (e). Another combination $A_4B_5C_1D_5E_4$ was developed and the results from this combination were in health agreement to the experimental ones.

Table 13. Comparison of ballistic performance

	Energy absorption (J)	Failure time of the first yarn broken (μs)	Number of failed yarns
$A_2B_5C_1D_5E_3$	18.84	49	1
$A_2B_5C_1D_5E_5$	17.92	44	1
$A_4B_5C_1D_5E_5$	16.26	--	None
$A_4B_5C_1D_5E_4$	14.09	37	2
Experiments	13.16(±1.2)	27.78 ~38.89	1 or 2

This is one way to identify a combination from the elastic constant values in the references, but it may lead to some bias during the selection of the optimal material properties. It is

possible to obtain other appropriate combinations by adjusting the parameters in other ways following the similar logic based on the understanding of each factor in the range analysis. Therefore, a more systematic approach should be further carried out to reduce or even eliminate the bias. However, the bias is principally existent in identifying the inferior influential factors including E_{11}, E_{33} and ν, and exists in the second influential (G_{23}) to some extents based on the analysis of their tendencies. For instance, it is not possible that G_{23} is higher than 1.50GPa. As the most influential factor, G_{13} in the present study could only be assigned to 0.37GPa. For the levels not considered in this study and higher than 0.37GPa, it is necessary to assign the G_{13} close to 0.37GPa to reflect the practical situation of Dyneema® yarn or fabrics at ballistic impact. For the levels lower than 0.37GPa, it is highly possible that other appropriate values of G_{13} could be identified to match the ballistic experiments too.

5 Discussions

5.1 Influence of other levels of the factors

The selection of the levels of the factors is based on the data used in the others' studies. According to the classical Smith theory [59], E_{11} is one of the most important parameters affecting ballistic performance of the material. It is reasonable to predict that the weight of the E_{11} would be changed when its level range is considerably extended. Chu *et al.* [49] presented the significant influence of the E_{11} in the range from 42.31GPa to 169.24GPa on the ballistic performance including energy absorption and yarn failure time, but the influence decreased when E_{11} is assumed to be 84.62GPa and 126.93GPa. Notably, the results presented in this research for E_{11} in Figures 6(a), 8(a) and 10(a) coincide with their conclusion that the energy absorption would increase as the E_{11} increases but sharply drop when it is high enough due to the earlier yarn failure. This enhances the significance of using the orthogonal method.

For other factors, it is reasonable to predict that their weight would not be significantly changed based on earlier studies [13-15], where the range of these factors was much wider but similar conclusions have been drawn that G_{13} is the most influential factor in terms of the energy absorption. In addition, according to the range analysis of G_{13} in Figures 6(d), 8(d) and 10(d), the outcomes became very sensitive when the G_{13} is lower than 1.50GPa. Hence, the weight of the G_{13} among all the elastic properties will decrease if the level range below 1.50GPa is not considered. Such an argument could also be supported by similar results from the work of Ha-Minh *et al.* [15].

5.2 Importance of G_{13} for materials under ballistic impact

The statistical analysis based on the orthogonal experiments identified G_{13} as the most influential yarn material property affecting all the performance indices, namely the energy absorption, failure time of the first yarn broken, and number of failed yarns. The importance of G_{13} could be attributed to the transverse loading to the ballistic material during the impact event. Supports to the claim can be found from numerous previous researches. Many [14, 37, 60-62] reported the importance of shear force on the yarn failure, implying the considerable influence of the shear modulus on the yarn failure. Wang *et al.* [63] and Smith *et al.* [64]

claimed that transverse stress wave of a yarn model caused by a ballistic impact is one of the most influential factors for energy absorption and stress distribution, and is highly correlated to its shear modulus [65][66]. In addition, G_{13} has been found to be the most significant elastic material property affecting the yarn de-crimping in FE modelling, hence the ballistic behaviour of the fabric model [19, 67].

6. Conclusion

This research aimed to identify the influence of each elastic constant on the ballistic performance of the Dyneema® fabric models with respect to energy absorption, failure time of the first yarn broken and number of failed yarns, and to find an appropriate combination for the elastic constants for Dyneema® yarns using the orthogonal experiment method based on Taguchi techniques. With a Dyneema® woven fabric model, an orthogonal table L_{25} (5^6) was developed with six factors and each of them has five levels. The range analysis and the analysis of variance (ANOVA) were employed for result discussions. The following conclusions are drawn from this research.

(1) For the Dyneema® yarn-based woven fabric model, when E_{11} is taken in the range 80GPa to 120GPa which is the normal range in published resources, G_{13} is at least more than twice as important as the other elastic constants, in terms of energy absorption, failure time of the first yarn broken and number of failed yarns, with more than 95% confident level. The reasons for its importance lie in the influence of G_{13} on the yarn failure, the transverse deflection of yarn model and the de-crimping of yarns. The value of G_{13} is usually taken in simulation by estimation due to difficulties in measuring it. The finding from this research illustrates it is critical of using a good estimation.

(2) The optimal combination of elastic constants for FE analysis of the Dyneema® fabrics has been identified to be $A_4B_5C_1D_5E_4$, leading to the simulated results that match the experimental results. This optimal values for the set of elastic constants are E_{11} = 90GPa, E_{33} = 0.37GPa, ν = 0, G_{13} = 0.37GPa, and G_{23} = 0.75GPa. It is believed that a more systematic approach is necessary for obtaining more accurate elastic properties of the Dyneema® yarn.

(3) This work confirmed that the orthogonal experiment method is a feasible methodology for weighting the influence of each elastic constant of yarn model on the ballistic performance of its fabric model in FE modelling and for identifying how important each factor is.

(4) The orthogonal experiment method can be used for identifying an appropriate combination of elastic constants with limited trials, the results of which are in well agreement to the experimental ones.

Acknowledgement

The authors wish to thank DSM for providing the Dyneema® yarns that used in the research.

Reference

1. Armstrong CG. *Modelling requirements for finite-element analysis*. Computer-aided design, 1994. **26**(7): p. 573-578.
2. Cunniff PM. *Dimensionless parameters for optimization of textile-based body armor systems*. In Proceedings of the 18th International and Symposium on Ballistics, 1999. pp. 1303-1310.
3. Huang W, Wang Y and Xia Y. *Statistical dynamic tensile strength of UHMWPE-fibers*. Polymer,2004. **45**(11): p. 3729-3734.
4. Koh ACP, Shim VPW and Tan VBC. *Dynamic behaviour of UHMWPE yarns and addressing impedance mismatch effects of specimen clamps*. International Journal of Impact Engineering, 2010. **37**(3): p. 324-332.
5. Russell B, Karthikeyan K, Deshpande VS and Fleck NA. *The high strain rate response of ultra high molecular-weight polyethylene: from fibre to laminate.* International Journal of Impact Engineering, 2013. **60**: p. 1-9.
6. Grujicic M, Arakere G, He T, Bell WC, Cheeseman BA, Yen CF and Scott B. *A ballistic material model for cross-plied unidirectional ultra-high molecular-weight polyethylene fiber reinforced armor-grade composites.* Materials Science and Engineering: A, 2008. **498**(1): p. 231-241.
7. Min S, Chu Y and Chen X. *Numerical study on mechanisms of angle-plied panels for ballistic protection.* Materials & Design, 2016. **90**: p. 896-905.
8. Zhou Y, Chen X and Garry W. *Influence of yarn gripping on the ballistic performance of woven fabrics from ultra-high molecular weight polyethylene fibre.* Composites Part B: Engineering, 2014. **62**: p. 198-204.
9. Chocron S, Kirchdoerfer T, King N and Freitas CJ. *Modeling of fabric impact with high speed imaging and nickel-chromium wires validation*. Journal of Applied Mechanics, 2011. **78**(5), 051007.
10. Wang Y, Chen X, Young R, Kinloch I and Garry W. *A numerical study of ply orientation on ballistic impact resistance of multi-ply fabric panels.* Composites Part B: Engineering, 2015. **68**: p. 259-265.
11. Kawabata S. *Measurement of the transverse mechanical properties of high-performance fibres.* Journal of the Textile Institute, 1990. **81**(4): p. 432-447.
12. Grujicic M, Arakere G, He T, Gogulapati M and Cheeseman BA. *A numerical investigation of the influence of yarn-level finite-element model on energy absorption by a flexible-fabric armour during ballistic impact.* Proceedings of the Institution of Mechanical Engineers, Part L: Journal of Materials Design and Applications, 2008. **222**(4): p. 259-276.
13. Nilakantan G. *Filament-level modeling of Kevlar KM2 yarns for ballistic impact studies.* Composite Structures, 2013. **104**: p. 1-13.
14. Sockalingam S, Gillespie JW and Keefe M. *Modeling the fiber length-scale response of Kevlar KM2 yarn during transverse impact*. Textile Research Journal, 2016. **87**(18), p. 2242-2254.
15. Ha-Minh C, Imad A, Boussu F, Kanit T and Crépin D. *Numerical study on the effects of yarn mechanical transverse properties on the ballistic impact behavior of textile fabric.* The Journal of Strain Analysis for Engineering Design, 2012. **47**(7): p. 524-534.
16. Komeili M and Milani AS. *The effect of meso-level uncertainties on the mechanical response of woven fabric composites under axial loading.* Computers & Structures, 2012. **90**: p. 163-171.
17. Komeili M and Milani AS. *Shear response of woven fabric composites under meso-level uncertainties.* Journal of composite materials, 2013. **47**(19): p. 2331-2341.
18. Akmar AI, Lahmer T, Bordas SPA, Beex LAA and Rabczuk T. *Uncertainty quantification of dry woven fabrics: A sensitivity analysis on material properties.* Composite Structures, 2014. **116**: p. 1-17.
19. Erol O, Powers BM and Keefe M. *Effects of weave architecture and mesoscale material properties on the macroscale mechanical response of advanced woven fabrics.* Composites Part A: Applied Science and Manufacturing, 2017. **101**: p. 554-566.

20. Wang Y, Chen X, Young R, Kinloch I and Garry W. *An experimental study of the effect of ply orientation on ballistic impact performance of multi-ply fabric panels.* Textile Research Journal, 2015. p. 34-43.
21. Rao MP, Duan Y, Keefe M, Powers BM and Bogetti TA. *Modeling the effects of yarn material properties and friction on the ballistic impact of a plain-weave fabric*. Composite Structures, 2009. **89**(4):p. 556-566.
22. Sockalingam S, Chowdhury SC, Gillespie JW and Keefe M. *Recent advances in modeling and experiments of Kevlar ballistic fibrils, fibers, yarns and flexible woven textile fabrics–a review.* Textile Research Journal, 2017. **87**(8): p. 984-1010.
23. Duan Y, Keefe M, Bogetti TA and Cheeseman BA. *Modeling friction effects on the ballistic impact behavior of a single-ply high-strength fabric*. International Journal of Impact Engineering, 2005. **31**(8): p. 996-1012.
24. Duan Y, Keefe M, Bogetti TA and Cheeseman BA. *Modeling the role of friction during ballistic impact of a high-strength plain-weave fabric*. Composite Structures, 2005. **68**(3): p. 331-337.
25. Duan Y, Keefe M, Bogetti TA, Cheeseman BA and Powers B. *A numerical investigation of the influence of friction on energy absorption by a high-strength fabric subjected to ballistic impact*. International Journal of Impact Engineering, 2006. **32**(8):p. 1299-1312.
26. Nilakantan G and Gillespie JW. *Ballistic impact modeling of woven fabrics considering yarn strength, friction, projectile impact location, and fabric boundary condition effects*. Composite Structures, 2012. **94**(12):p. 3624-3634.
27. Talebi H, Wong SV and Hamouda AMS. *Finite element evaluation of projectile nose angle effects in ballistic perforation of high strength fabric.* Composite Structures, 2009. **87**(4): p. 314-320.
28. Shanahan W and Hearle J. *An Energy method for calculations in fabric mechanics PartII: Examples of Application of the method to woven fabrics*. Journal of the textile institute, 1978. **69** (4):p. 92-100
29. Valizadeh M, Lomov S, Ravandi SAH, Salimi M and Rad SZ. *Finite element simulation of a yarn pullout test for plain woven fabrics.* Textile Research Journal, 2010. **80**(10): p. 892-903.
30. Chen X, Zhou Y and Garry W, *Numerical and experimental investigations into ballistic performance of hybrid fabric panels.* Composites Part B: Engineering, 2014. **58**: p. 35-42.
31. Yang CC, Ngo T and Tran P. *Influences of weaving architectures on the impact resistance of multi-layer fabrics.* Materials & Design, 2015. **85**: p. 282-295.
32. Ha-Minh C, Kanit T, Boussu F and Imad A. *Numerical multi-scale modeling for textile woven fabric against ballistic impact.* Computational Materials Science, 2011. **50**(7): p. 2172-2184.
33. Gebreyohaness AS, Clifton GC and Butterworth JW. *Finite element modeling of non-ductile RC walls.*15th World Conference on Earthquake Engineering (15WCEE), 2012. **38**(9): p. 3320-3329.
34. Abaqus Analysis User's Manual. Ed. 6.10 V. 2010 Availalbe at: http://130.149.89.49:2080/v6.10ef/books/usb/default.htm?startat=pt06ch24s01aus102.html. Last access data: 20th-April-2018.
35. Abdulhamid H, Kolopp A, Bouvet C and Riballant S. *Experimental and numerical study of AA5086-H111 aluminum plates subjected to impact.* International Journal of Impact Engineering, 2013. **51**: p. 1-12.
36. Henninger HB, Reese SP, Anderson AE and Weiss JA. *Validation of computational models in biomechanics.* Proceedings of the Institution of Mechanical Engineers, Part H: Journal of Engineering in Medicine, 2010. **224**(7): p. 801-812.
37. Sockalingam S, Gillespie JW and Keefe M. *Dynamic modeling of Kevlar KM2 single fiber subjected to transverse impact.* International Journal of Solids and Structures, 2015. **67**: p. 297-310.
38. Roy RK. *Design of experiments using the Taguchi approach: 16 steps to product and process improvement*. John Wiley & Sons; 2001. p. 98-102.

39. Roy RK. *Design of experiments using the Taguchi approach: 16 steps to product and process improvement*. John Wiley & Sons; 2001. p. 217-220.
40. Wu X and Leung D Y. *Optimization of biodiesel production from camelina oil using orthogonal experiment*. Applied Energy, 2011. **88**(11), 3615-3624.
41. Tang J, Gong G, Su H, Wu F and Herman C. *Performance evaluation of a novel method of frost prevention and retardation for air source heat pumps using the orthogonal experiment design method*. Applied Energy, 2016. **169**: p. 696-708.
42. Sanborn B, DiLeonardi AM and Weerasooriya T. *Tensile properties of Dyneema SK76 single fibers at multiple loading rates using a direct gripping method.* Journal of Dynamic Behavior of Materials, 2015. **1**(1): p. 4-14.
43. Attwood JP, Fleck NA, Wadley HNG and Deshpande VS. *The compressive response of ultra high molecular weight polyethylene fibres and composites.* International Journal of Solids and Structures, 2015. **71**: p. 141-155.
44. Hudspeth M, Nie X and Chen W. *Dynamic failure of Dyneema SK76 single fibers under biaxial shear/tension.* Polymer, 2012. **53**(24): p. 5568-5574.
45. http://www.pelicanrope.com/pdfs/Dyneema-Comprehensive-factsheet-UHMWPE.pdf. Last access data: 21st-Nov-2016
46. Heru Utomo B. *High-speed impact modelling and testing of dyneema composite*. PhD thesis, Delft University of Technology; 2011. p. 88-89.
47. Chu Y, Chen X, and Tian L. *Modifying friction between ultra-high molecular weight polyethylene (UHMWPE) yarns with plasma enhanced chemical vapour deposition (PCVD).* Applied Surface Science, 2017. **406**: p. 77-83.
48. Chu Y. *Surface modification to aramid and UHMWPE fabrics to increase inter-yarn friction for improved ballistic performance.* PhD thesis, University of Manchester; 2015. p. 105-139.
49. Chu TL, Ha-Minh C and Imad A. *A numerical investigation of the influence of yarn mechanical and physical properties on the ballistic impact behavior of a Kevlar KM2® woven fabric.* Composites Part B: Engineering, 2016. **95**: p. 144-154.
50. Roy RK. *Design of experiments using the Taguchi approach: 16 steps to product and process improvement*. John Wiley & Sons; 2001. p. 338-339.
51. Rao MP, Nilakantan G, Keefe M, Powers BM and Bogetti TA. *Global/local modeling of ballistic impact onto woven fabrics.* Journal of composite materials, 2009. **43**(5): p. 445-467.
52. Peijs AA and De Kok JM. *Hybrid composites based on polyethylene and carbon fibres. Part 6: Tensile and fatigue behaviour.* Composites, 1993. **24**(1): p. 19-32.
53. Lv L and Gu B. *Transverse impact damage and energy absorption of three-dimensional orthogonal hybrid woven composite: Experimental and FEM simulation.* Journal of composite materials, 2008. **42**(17): p. 1763-1786.
54. Roy RK. *Design of experiments using the Taguchi approach: 16 steps to product and process improvement*. John Wiley & Sons; 2001. p. 207-209.
55 Zhou L, Shi W and Wu S. *Performance optimization in a centrifugal pump impeller by orthogonal experiment and numerical simulation*. Advances in Mechanical Engineering, 2013. 5: 385809.
56. Roy RK. *Design of experiments using the Taguchi approach: 16 steps to product and process improvement*. John Wiley & Sons; 2001. p. 213-214.
57. Roy RK. *Design of experiments using the Taguchi approach: 16 steps to product and process improvement*. John Wiley & Sons; 2001. p. 231-232.
58. Ross PJ. *Taguchi techniques for quality engineering: loss function, orthogonal experiments, parameter and tolerance design*. New York: McGraw-Hill; 1988. p. 288-289.
59. McCrackin FL, Schiefer HF, Smith JC and Stone WK. *Stress-strain relationships in yarns subjected to rapid impact loading: Part II. Breaking velocities, strain energies, and theory neglecting wave propagation.* Textile Research Journal, 1955. **25**(6): p. 529-534.

60. Chen X, Zhu F, and Garry W. *An analytical model for ballistic impact on textile based body armour.* Composites Part B: Engineering, 2013. **45**(1): p. 1508-1514.
61. Naik NK and Shrirao P. *Composite structures under ballistic impact.* Composite Structures, 2004. **66**(1-4): p. 579-590.
62. Carr DJ. *Failure mechanisms of yarns subjected to ballistic impact.* Journal of materials science letters, 1999. **18**(7): p. 585-588.
63. Wang Y, Chen X, Young R and Kinloch I. *Finite element analysis of effect of inter-yarn friction on ballistic impact response of woven fabrics.* Composite Structures, 2016. **135**: p. 8-16.
64. Smith JC, Blandford JM, and Schiefer HF. *Stress-Strain Relationships. in Yarns Subjected to Rapid Impact Loading: Part VI: Velocities of Strain Waves Resulting from Impact.* Textile Research Journal, 1960. **30**(10): p. 752-760.
65. Gere JM and Goodno BJ. *Mechanics of materials. cengage learning toronto; 2009.* Chap **3**: p. 249-250.
66. Gere JM and Goodno BJ. *Mechanics of materials. cengage learning toronto; 2009.* Chap **5**: p. 392-393.
67. Erol O and Keefe M. *Numerical modeling techniques for woven textiles.* SAMPE Tech Seattle 2014 Conference.